International Journal of Environmental Science and Technology
https://doi.org/10.1007/s13762-021-03610-w

ORIGINAL PAPER

# Copper(II) and lead(II) adsorption onto zinc sulfide nanoparticles effects of light, pH, time, temperature, and interferences

J. M. Cantu[1] · J. P. Valle[1] · A. Puente[1] · C. Valdes[1] · K. Flores[1] · H. M. Morales[1] · E. Fletes[2] · M. Alcoutlabi[2] · E. Kotsikorou[1] · J. G. Parsons[1]

Received: 8 May 2021 / Revised: 26 July 2021 / Accepted: 12 August 2021
© Islamic Azad University (IAU) 2021

**Abstract**
A ZnS nano-sorbent to remove copper(II) and lead(II) ions from aqueous solutions was prepared via a hydrothermal reaction and characterized by X-ray diffraction. The zinc sulfide nanoparticle size was determined to be $7.0 \pm 0.22$ nm. The effects of pH, light conditions, time, capacity, and interferences on the zinc sulfide ability to remove copper(II) and lead(II) ions from aqueous solutions were investigated. pH studies showed that pH 5 was the optimal value for zinc sulfide binding both copper(II) and lead(II) ions. Under ambient light, the binding of both ions occurred within the first 5 min. Binding capacities ranged from 116.2 to 243.9 mg/g for copper(II), 39.1 to 147.1 mg/g for lead(II) ions, and 36.1–79.4 mg/g for lead(II) ions in the dark over temperature range from 4 to 45 °C. The thermodynamic parameters showed that the binding process for both copper(II) and lead(II) ions was either spontaneous or close to equilibrium. Light conditions were also investigated in the context of cation interference and showed that the presence of hard cations had no effect on the binding of lead(II) ions. On the other hand, the presence of hard cations showed small decrease in the binding of copper(II) ions.

**Keywords** Adsorption · Zinc sulfide · Lead · Copper · Metal binding

## Introduction

Anthropogenic materials such as petroleum by-products, herbicides, pesticides, and heavy metal ions are known to cause contamination of drinking water (Fujii et al. 2007; Tahoon et al. 2020). Heavy metal ions are classified as non-biodegradable substances, which are toxic in high concentrations. Copper(II) ($Cu^{2+}$) and lead(II) ($Pb^{2+}$) ions are two heavy metal ions of interest due to the health implications from exposure (Santucci and Scully 2020; Taylor et al. 2020). $Cu^{2+}$ is classified as an essential trace element, which is required in small amounts, for biological purposes including the correct growth and development of organisms (Gaetke and Chow 2003). However, the consumption of high amounts of copper can lead to disruptions in the nervous system, abdominal pain, liver toxicity, diarrhea, anorexia, and lethargy in humans (Georgopoulos et al. 2006; Mosayebi and Azizian 2016; Tamez et al. 2016; Wu et al. 2013). On the other hand, lead has no beneficial biological purpose in the growth and development of mammals. Lead commonly exists as a divalent cation at low concentrations and has been known to compete with the binding of calcium to phosphokinase C (PKC), thus affecting neural signaling and cellular uptake of $Ca^{2+}$ (Needleman 2004). A high amount of $Pb^{2+}$ in the human body has been shown to affect the nervous and renal systems, and the production of hemoglobin. The exposure of children to $Pb^{2+}$ during developmental stages is considered high risk since they absorb $Pb^{2+}$ 4 to 5 times more readily than adults (Tong et al. 2000; WHO 2003). Thus, there is a need to develop technologies to remove both $Cu^{2+}$ and $Pb^{2+}$ from drinking waters.

Many remediation techniques have been used for the removal of both $Cu^{2+}$ and $Pb^{2+}$ from aqueous solutions including but not limited to the following technologies: ion exchange, precipitation, biosorption, reverse osmosis,

Editorial responsibility: Maryam Shabani.

✉ J. G. Parsons
jason.parsons@utrgv.edu

[1] Department of Chemistry, University of Texas Rio Grande Valley, 1 West University Blvd., Brownsville, TX 78521, USA

[2] Department of Mechanical Engineering, University of Texas Rio Grande Valley, 1201 W University Blvd., Edinburg, TX 78539, USA

Published online: 21 August 2021

phytoremediation, and adsorption (Barlokova et al. 2019; Fu and Wang 2011). Several of these methods have proven to be effective in the removal of heavy metal ions; however, many of these methods are either too difficult to implement or too expensive. For instance, ion exchange resins typically are not ion specific and tend to coordinate to all cations in solution. Precipitation involves the use of precipitating agents, which requires additional treatment of water to remove excess chemicals (Fu and Wang 2011). However, adsorption has attracted attention for the remediation of heavy metal ions using materials such as granular ferric oxide (GFO) and modified GFO (Barlokova et al. 2019; Li et al. 2020; Streat et al. 2008). Recently, research efforts have focused on the use of nanosized adsorbents with high surface areas and reactivities, which have exhibited higher binding capacities than non-nanosized materials.

Over the years, different nano-adsorbents have been investigated for the remediation of heavy metals from aqueous solutions (Alghamdi et al. 2019; Anthemidis and Ioannou 2009; Harsha Vardhan et al. 2020; Kaushal and Singh 2017; Kovacova et al. 2019; Luo et al. 2021; Sarma et al. 2019; Shahabuddin et al. 2018; Shahin et al. 2019; Yang et al. 2019). Inorganic metal-oxide nanomaterials have shown much promise for the remediation of $Cu^{2+}$ and $Pb^{2+}$ from water solutions. For example, Tamez et al. (2016) showed that $Fe_2O_3$ exhibited binding capacities for $Cu^{2+}$ and $Pb^{2+}$ of 19.61 and 47.62 mg/g, respectively (Tamez et al. 2016). Tamez et al. also showed that $Fe_3O_4$ had higher binding capacities for the sorption of $Cu^{2+}$ and $Pb^{2+}$ at 37.04 and 166.67 mg/g, respectively. The binding capacities of $TiO_2$, determined by Mahdavi et al. were 50.2 and 21.7 mg/g for both $Cu^{2+}$ and $Pb^{2+}$, respectively (Mahdavi et al. 2013). In a different study, Mahdavi et al. investigated the sorption of $Pb^{2+}$ and $Cu^{2+}$ by ZnO and CuO nanoparticles, and determined that ZnO had high binding capacities of 112.7 and 137.5 mg/g for $Pb^{2+}$ and $Cu^{2+}$ while CuO exhibited relatively low binding capacities for $Pb^{2+}$ and $Cu^{2+}$, 14.2 and 54.1 mg/g, respectively (Mahdavi et al. 2012). In another study, $\gamma$-$Al_2O_3$ showed a similar binding capacity for the sorption of $Cu^{2+}$, which was 51.3 mg/g at 25 °C (Fouladgar et al. 2015). Other adsorbents that have been used include manganese oxides, graphene oxides, red mud, and tin oxides (Ahmad et al. 2009; Azzam et al. 2016; Farghali et al. 2013; Liu et al. 2016; Mosayebi and Azizian 2016; Sitko et al. 2013; Wang et al. 2015a, 2015b; Zepeda et al. 2018). However, the investigation of $Cu^{2+}$ and $Pb^{2+}$ adsorption to transition metal sulfides has been somewhat limited in scope. However, Wang et al. studied the adsorption of $Pb^{2+}$ ions onto disulfide cross-linked poly(methacrylic acid) iron oxide nanoparticles, which had a binding capacity of 48.7 mg/g (Wang et al. 2021). Qu et al. investigated $Pb^{2+}$ binding to carbon-supported sulfide nZVI, which showed a binding capacity of 295.30 mg/g (Qu et al. 2021).

In the current study, zinc sulfide (ZnS) was synthesized and investigated for the absorption of both $Cu^{2+}$ and $Pb^{2+}$ from aqueous solutions. The nano-sorbent was synthesized via a hydrothermal process using a mixture of 60 mmol of $Zn(NO)_3$ and 60 mmol $Na_2S{\cdot}9H_2O$ in 18MΩ $H_2O$. The solution mixture was reacted in a Teflon-lined autoclave at 150 °C for 3 h. The nano-sorbent was characterized using powdered X-ray diffraction (XRD), which confirmed a cubic crystal structure with an average particle size of $7.0 \pm 0.22$ nm as determined using Scherrer's equation. XRD analysis was performed after the reaction of ZnS with the $Cu^{2+}$ and $Pb^{2+}$. Various batch studies were performed to determine the effects of pH, temperature, time, common cationic interferences, and thermodynamics for the binding processes of $Cu^{2+}$ and $Pb^{2+}$. Batch isotherm studies were performed to determine the binding capacities of the synthesized ZnS nanoparticles. Furthermore, the effects of ambient light, UV light, and absence of light (dark) on the sorption process were investigated. The experiments were performed between 2018 and 2019 in the Department of Chemistry, at the University of Texas Rio Grande Valley, Texas, USA.

## Materials and methods

### Materials

Zinc nitrate ($Zn(NO_3)_2{\cdot}6H_2O$), sodium sulfide ($Na_2S{\cdot}9H_2O$), copper nitrate ($Cu(NO_3)_2{\cdot}2.5\ H_2O$), and lead nitrate ($Pb(NO_3)_2$) were purchased from Sigma-Aldrich. Ultra-pure water (with a resistance of 18 Ω) was obtained from a Millipore Milli-Q Plus water filtration system. Standard stock solutions of $Cu^{2+}$ and $Pb^{2+}$ were prepared in ultra-pure water using $Cu(NO_3)_2{\cdot}2.5H_2O$ and $Pb(NO_3)_2$ salts, respectively. The pH of all solutions was adjusted using either dilute trace metal-grade nitric acid ($HNO_3$) or dilute sodium hydroxide solution (NaOH).

### Synthesis of ZnO nanoparticles

The synthesis of ZnS nanoparticles was performed using a similar method to that reported by (Hoa et al. 2009). In brief, 60 mmol of both zinc nitrate ($Zn\ (NO_3)_2{\cdot}6\ H_2O$) and sodium sulfide ($Na_2S{\cdot}9H_2O$) were each dissolved in 60 mL of ultra-pure water. The $Zn(NO_3)_2{\cdot}6H_2O$ was titrated with $Na_2S{\cdot}9H_2O$ dropwise over a period of 1 h. The final mixture was transferred to Teflon-lined autoclaves and reacted at 150 °C for 3 h. After autoclaving, the sample was cooled naturally to room temperature and the precipitate was collected, centrifuged, and washed five times with ultra-pure water to remove any by-products formed during the reaction. The precipitate was then dried overnight under vacuum at room temperature prior to analysis.

## Characterization of ZnS nanoparticles

The ZnS nano-adsorbent was characterized using XRD to determine the phase and crystallite size. The ZnS nanomaterial was homogenized using a mortar and pestle and finally placed on an Al sample holder. The XRD analysis was performed using a Rigaku Miniflex II diffractometer equipped with a Cu source ($K\alpha = 1.54$ Å), a nickel filter, and a scintillation counter detector. The XRD patterns were collected from 20° to 60° in $2\theta$ using a step width of 0.05° and a counting time of 5 s. The average particle size was determined using a Gaussian fitting of three diffraction peaks and Scherer's equation. The crystal fitting was performed using the Le Bail fitting procedure in the FullProf Suite of Software and crystallographic data from the literature (Rodriguez-Carvajal 1993; Berry 1954; Cantu et al. 2018; Evans and Konnert, 1976; Hoa et al. 2009; Kiflawi et al. 1969; Ma et al. 2016; Mardix et al. 1967; Oftedal 1932; Sadovnikov and Rempel 2009; Salavati-Niasari et al. 2012; Wang et al. 2013; Yin et al. 2016).

## pH studies

The determination of the optimal pH for adsorption was performed using batch adsorption experiments. pH profiles were performed in triplicate under ambient light, UV light, and no light. The pH of standard stock solutions of 0.3 ppm of $Cu^{2+}$ and 0.3 mM $Pb^{2+}$ was adjusted from a range of pH 2 to 6. In a test tube, 10 mg of ZnS was mixed with a 4 mL aliquot of each pH-adjusted standard solution. Control test tubes consisted of only $Pb^{2+}$ or $Cu^{2+}$ ion solutions without the ZnS nanoparticles were treated the same as the reaction samples. The samples were equilibrated for 1 h at room temperature on a nutating mixer. After equilibration, the test tubes were centrifuged at 3500 rpm for 5 min while the supernatants were decanted and stored for inductively coupled plasma optical emission (ICP-OES) analysis.

## Time dependency and kinetics studies

The effect of time on the adsorption and activation energies for the binding of $Cu^{2+}$ and $Pb^{2+}$ with the ZnS nano-adsorbent was studied by batch experiments. The pH of standard stock solutions of 30 ppm of $Cu^{2+}$ and 0.3 mM $Pb^{2+}$ was adjusted to the optimal binding pH 5. The experiments were performed in test tubes using 10 mg of ZnS and 4-mL aliquots of adjusted stock solutions. The control test tubes consisted of only the $Pb^{2+}$ or $Cu^{2+}$ ion solutions without the ZnS nanoparticles were treated the same as the reaction samples. The batch experiments were prepared in triplicate and equilibrated for time intervals of 5, 10, 15, 30, 60, 90, 120, and 240 min at temperatures of 4, 22, and 45 °C. After equilibration, the samples were centrifuged at 3500 rpm for 5 min while the supernatants were decanted and stored ICP-OES analysis.

## Adsorption isotherms

The batch adsorption isotherm studies were performed to determine the binding capacities and thermodynamics of the binding of both $Cu^{2+}$ and $Pb^{2+}$ with ZnS under both ambient light and no light. Standard stock solutions of $Cu^{2+}$ and $Pb^{2+}$ of 0.3, 3, 30, 100, 300, and 1000 ppm were adjusted to the optimal binding pH 5. The batch experiments were performed in test tubes using 10 mg of ZnS and aliquots of 4 mL of adjusted stock solutions. Control test tubes consisted of only the $Pb^{2+}$ or $Cu^{2+}$ solution with no ZnS nanoparticles were treated the same as the reaction samples. The batch experiments were prepared in triplicate and equilibrated for 1 h on a nutating mixer at temperatures of 4, 22, and 45 °C. The samples were centrifuged at 3500 rpm for 5 min. The supernatants were then decanted and stored in clean test tubes for further analysis via ICP-OES.

## Interference study

The binding interferences were tested for the effects on the sorption of $Cu^{2+}$ and $Pb^{2+}$ in the presence of common hard cations in ambient light and no light conditions. The cations used in the study were $Na^{+}$, $K^{+}$, $Ca^{2+}$, and $Mg^{2+}$ at 0.3, 3, 30, 100, 300, and 1000 ppm. In addition, the interference was also investigated using a solution consisting of all the interferences combined in a single solution. Standard stock solutions of 0.3 ppm of $Cu^{2+}$ and 0.3 mM $Pb^{2+}$ were adjusted to the optimum binding pH 5. The batch experiments were performed in triplicate in test tubes containing ZnS and aliquot of each adjusted stock solution. The aliquot volume and sorbent mass used for each respective condition are shown in Table 1. The control test tubes consisted of the $Pb^{2+}$ or $Cu^{2+}$ solution without ZnS nanoparticles were treated the same as the reaction samples. The samples were equilibrated for 1 h at room temperature on a nutating mixer. After equilibration, the reaction and control tubes were centrifuged, and the supernatants were decanted and stored for further analysis using ICP-OES.

**Table 1** Sample contents for the sorption of $Cu^{2+}$ and $Pb^{2+}$ with the ZnS nano-sorbent under different light conditions

| Light conditions | Aliquot volume (mL) | Sorbent mass (mg) |
|---|---|---|
| Ambient | 4 | 10 |
| Dark | 4 | 10 |
| UV | 8 | 20 |

**Table 2** Parameters used for ICP-OES analysis using a PerkinElmer Optima 8300 ICP-OES for the analysis of $Cu^{2+}$ and $Pb^{2+}$ binding to ZnS

| Parameter | Settings |
|---|---|
| $\lambda_{Cu}$ | 327.393 nm |
| $\lambda_{Pb}$ | 217 nm |
| RF power | 1500 W |
| Nebulizer | Gemcone (low flow) |
| Plasma flow | 15 L/min |
| Auxiliary flow | 0.2 L/min |
| Nebulizer flow | 0.55 L/min |
| Sample flow | 1.50 mL/min |
| Injector | 2.0 mm Alumina |
| Spray chamber | Cyclonic |
| Integration time | 20 s |
| Replicates | 3 |

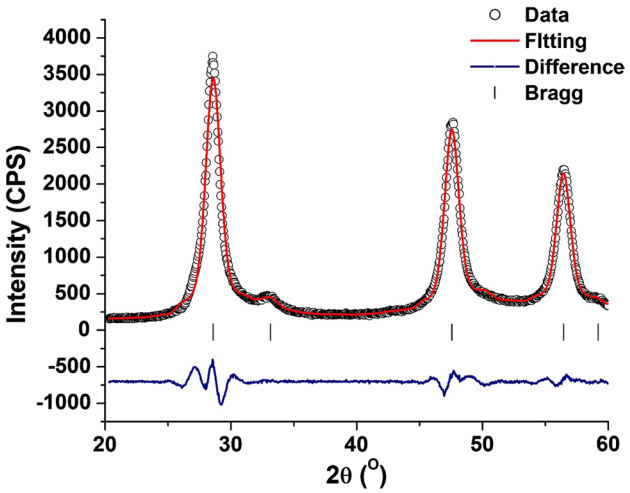


**Fig. 1** Le Bail fitting of the XRD pattern for the as-synthesized ZnS nanoparticles

## Sample analysis

The residual metal-ion concentration was determined using ICP-OES. The samples were analyzed after each sorption reaction using a PerkinElmer Optima 8300 ICP-OES (Shelton CT) using the Winlab32 software. The instrument parameters used are given in Table 2. The obtained calibration curves had correlation coefficients of ($R^2$) 0.99 or higher for the analysis of all $Cu^{2+}$ and $Pb^{2+}$ sample solutions. Any samples outside the calibration range of the ICP-OES were diluted and reexamined.

## Results and discussion

### X-ray diffraction

Figure 1 shows the diffraction pattern collected for the synthesized ZnS nano-sorbent. The synthesized ZnS nanoparticles had a cubic crystal structure with space group of F-43 M as determined for the fitting of the sample. The results of the fitting are shown in Table 3, which show the refined lattice parameters for the fitting were: $a=b=c=5.406$ Å and $\alpha=\beta=\gamma=90°$. In addition, the $\chi^2$ of the fitting was 1.78, which indicates a good agreement between the data and the reported results on the crystal structure (Hoa et al. 2009; Ma et al. 2016; Sadovnikov and Rempel 2009; Wang et al. 2013; Yin et al. 2016). The average particle size of the ZnS nano-sorbent was calculated to be $7.0 \pm 0.22$ nm using Scherrer's equation as shown below:

$$d = \frac{0.9\lambda}{B\cos\frac{2\theta}{2}} \quad (1)$$

where $d$ is the diameter or crystallite size, 0.9 is a correction factor for the Gaussian fitting, $\lambda$ is the wavelength for the Cu $K_\alpha = 1.54$ Å, $B$ is the full width half maximum (FWHM) of the diffraction peak, and cos $2\theta/2$ is the position of the diffraction peak. The average crystallite size was based on the three most prominent diffraction peaks in the pattern, which were the 111, 220, and 311 diffraction planes.

Figure 2 shows the diffraction patterns of ZnS nanoparticles after reaction with the $Cu^{2+}$ and $Pb^{2+}$ ions. In addition, Table 4 shows the results of the Le Bail fitting of the samples. Figure 2A shows the ZnS after reaction with lead nitrate at room temperature as can be seen the diffraction patterns changed from that of the pure ZnS. The sample turned black after the reaction indicating a change. From the diffraction pattern, the sample was determined to consist of two phases, which were identified as ZnS (cubic) and PbS in a galena-type material (cubic). The results of the fitting are shown in Table 4, which indicate a good fitting of the experimental data reported in the literature determined parameters of PbS and ZnS with a $\chi^2$ of 1.19, which shows a good agreement between the experimental results and those reported in the literature (Sadovnikov and Rempel 2009; Salavati-Niasari et al. 2012). The ZnS XRD pattern was observed to have the F-43 M space group with lattice parameters consistent with pure ZnS (Hoa et al. 2009; Ma et al. 2016; Sadovnikov and Rempel, 2009; Wang et al. 2013; Yin et al. 2016). Figure 2B shows the diffraction pattern for the product from the $Cu^{2+}$ reaction with the ZnS. The diffraction pattern only indicates the presence of the ZnS in the same phase as the unreacted ZnS with lattice parameters consistent with those observed in the literature, shown in Table 4 (Hoa et al. 2009; Ma et al. 2016; Sadovnikov and Rempel 2009; Wang et al. 2013; Yin et al. 2016). The reaction of Pb ions with the ZnS at elevated temperature (45 °C) resulted

**Table 3** Le Bail fitting results of the as-synthesized ZnS nanoparticles

| Sample | Space group | $a$(Å) | $b$(Å) | $c$(Å) | $\alpha$(°) | $\beta$(°) | $\gamma$(°) | $\chi^2$ |
|---|---|---|---|---|---|---|---|---|
| ZnS | F-4 3 m | 5.406(3) | 5.406(3) | 5.406(3) | 90.00 | 90.00 | 90.00 | 1.78 |

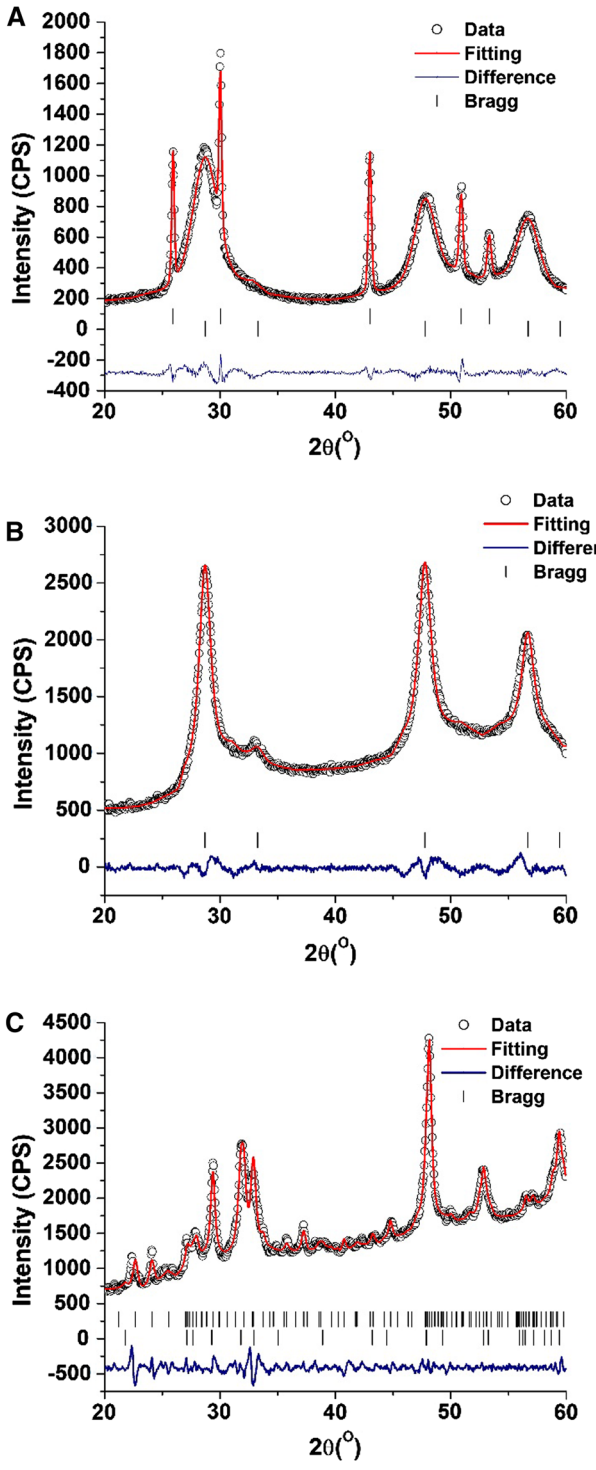


**Fig. 2** Le Bail fittings of the X-ray diffraction pattern for the ZnS nanoparticles after the reaction with $Pb^{2+}$ at room temperature (**a**), $Cu^{2+}$ ions at room temperature (**b**) and $Cu^{2+}$ at 45 °C (**c**)

in a solid phase, which looked like the sample prepared at room temperature. The reaction of the copper ions with the ZnS at an elevated temperature (45 °C) also resulted in a black/gray solid. The diffraction pattern of the $Cu^{2+}$ reaction with ZnS at elevated temperature is shown in Fig. 2C and the Le Bail fitting parameters are given in Table 4. The fitting of the ZnS–Cu sample showed a good agreement between the fitting and the diffraction data as indicated by the $\chi^2$ value of 2.29. The results of the fitting showed a change in the ZnS phase and the addition of a CuS phase. The ZnS crystal structure was converted from the cubic phase into the hexagonal phase with a space group of P3M1 and the lattice parameters were consistent with those reported in the literature (Kiflawi et al. 1969; Mardix et al. 1967). The results also showed the presence of a CuS phase in a hexagonal lattice P63/MMC with parameters consistent with the covellite phase of CuS (Berry 1954; Evans and Konnert 1976; Oftedal 1932). The formation of the lead and copper sulfides do have different formation constants and thermodynamics for their formation. The formation of PbS was observed at room temperature while the formation of CuS was only observed at high temperature, which was due to the thermodynamics of formation of Pbs and CuS. The $\Delta G°_f$ for $Cu^{2+}$ and $Pb^{2+}$ sulfides were − 53.6 kJ/mol and − 98.7 kJ/mol, respectively, which indicated the formation of PbS was more favorable than that of CuS (Lide 1994). In addition, the $\Delta S°_f$ of PbS and CuS were 91.2 J/mol and 66.5 J/mol, which again showed that formation of the PbS was favored over the CuS. Thus, it was not surprising to see that PbS was only formed at lower temperatures while the formation of CuS was observed at higher temperatures.

## pH profile studies

Figure 3 shows the results of the batch pH studies under ambient light for both the $Cu^{2+}$ and $Pb^{2+}$ ions. As can be seen in Fig. 3, the binding of $Cu^{2+}$ onto ZnS initially was low at pH 2, approximately 80%. At pH 3, the binding of $Cu^{2+}$ increased to approximately 90% and remained constant thereafter up to pH 6. However, the adsorption of $Pb^{2+}$, as can be seen in Fig. 3, was pH independent throughout the pH range used in the study. The binding of $Pb^{2+}$ at pH 2 was approximately 100% and remained unaffected as the pH of the solution increased to pH 6. From the results in Fig. 3, pH 5 was chosen as the optimal pH for further studies for both ions. Though pH 6 yielded similar results, it was not chosen for further studies due to the possible formation of the metal hydroxides $Cu(OH)_2$ and $Pb(OH)_2$, species which can be

**Table 4** Le Bail fitting of ZnS nanoparticles after reactions with $Pb^{2+}$ and $Cu^{2+}$ in light conditions and the binding of $Cu^{2+}$ under light conditions at elevated temperature

| Sample | Phase | Space group | *a*(Å) | *b*(Å) | *c*(Å) | *α*(°) | *β*(°) | *γ*(°) | $\chi^2$ |
|---|---|---|---|---|---|---|---|---|---|
| Pb–ZnS | Zn–S | F-43 M | 5.373(3) | 5.373(3) | 5.373(3) | 90.00 | 90.00 | 90.00 | 1.19 |
| | Pb–S | FM3M | 5.934(3) | 5.934(3) | 5.934(3) | 90.00 | 90.00 | 90.00 | |
| Cu–ZnS 21 °C | Zn–S | F-43 M | 5.406(3) | 5.406(3) | 5.406(3) | 90.00 | 90.00 | 90.00 | 1.78 |
| Cu–ZnS 45 °C | ZnS | P3M1 | 3.808(3) | 3.808(3) | 62.762(8) | 90.00 | 90.00 | 120.0 | 2.29 |
| | CuS | P63/MMC | 3.796(7) | 3.796(7) | 16.309(9) | 90.00 | 90.00 | 120.0 | |

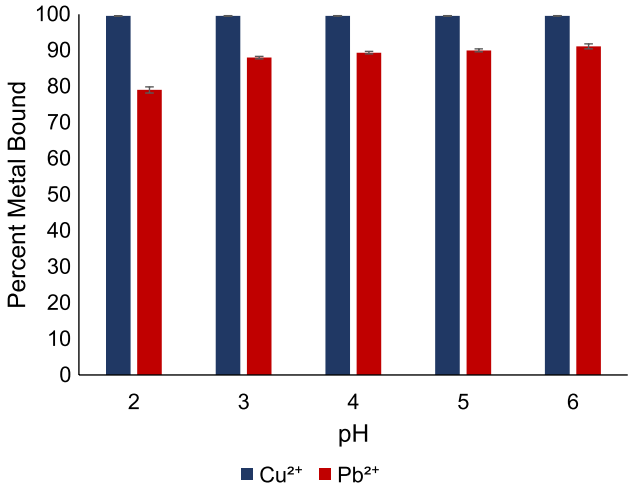


**Fig. 3** A batch pH profile study for the binding of $Cu^{2+}$ and $Pb^{2+}$ with ZnS in ambient light

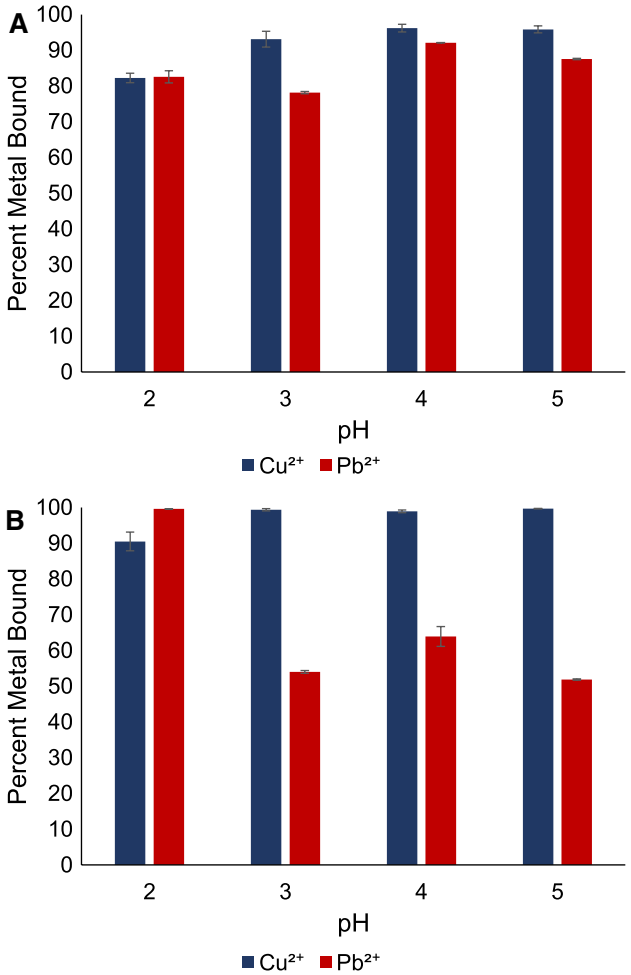


**Fig. 4** A pH profile studies for the sorption of both $Cu^{2+}$ and $Pb^{2+}$ with ZnS nanoparticles under UV lighting (**a**) and dark conditions (**b**)

observed at high concentrations. Due to the photocatalytic properties of ZnS, the batch pH studies were also performed in the absence of light (dark) and under UV light to determine whether the light-induced effects on the binding of $Pb^{2+}$ and $Cu^{2+}$ could be observed. Figure 4a and b shows the results for the binding of both $Cu^{2+}$ and $Pb^{2+}$ ions under UV light and dark conditions, respectively. As seen in Fig. 4a, the binding of both $Cu^{2+}$ and $Pb^{2+}$ were approximately 80% initially and remained above 80% binding throughout all pH values tested. The results were similar to those observed during the pH study using ambient light conditions. Both ions showed low binding at pH 2 which increased at pH 3 and remained relatively constant thereafter. The sorption of $Cu^{2+}$ onto ZnS under the dark reaction conditions (Fig. 4B) followed the same trend as was observed for the sorption of $Cu^{2+}$ under both the ambient and UV-light reaction conditions. However, as can also be seen in Fig. 4b, the sorption of $Pb^{2+}$ under the dark reaction conditions showed a decrease in the binding as the pH of the solution was increased. More specifically, the binding of $Pb^{2+}$ at pH 2 was observed to be approximately 100% and decreased to approximately 50% at pH 3, and the binding remained relatively constant through pH 5. For the pH studies with UV light and dark conditions, pH 5 was the highest pH studied, which was observed to be the optimal binding pH under ambient light conditions. In addition, at pH 6, there was the possibility of $Pb^{2+}$ precipitating due to the formation of $Pb(OH)_2$ species. The $Cu^{2+}$ ion adsorption under both the UV light and dark studies showed no significant effects on the binding, and thus, the light effects on $Cu^{2+}$ binding were not investigated any further. The UV light had a small effect on the binding of the $Pb^{2+}$ ions onto ZnS while the UV study was excluded from further investigation. The results obtained from the batch pH study were in agreement with the results reported in the literature (Ahmad et al. 2009; Farghali et al. 2013; Mahdavi

et al. 2012, 2013; Sitko et al. 2013; Tamez et al. 2016; Wang et al. 2015a; Wu et al. 2013). For example, the sorption of $Cu^{2+}$ and $Pb^{2+}$ onto pristine biochar showed an increase in binding as the pH of the solution increased. It increased from 20 to 90% binding as pH increased from 2 to 7, respectively (Azzam et al. 2016). In a different study, the sorption of both ions using engineered biochar removed 100% of $Cu^{2+}$ and $Pb^{2+}$ at pH 7 (Wang et al. 2015). Similarly, the binding of $Cu^{2+}$ to graphene oxide nanomaterial has shown an increase in binding as the initial pH of the solution increased from 1 to 7 (Wu et al. 2013). Mahdavi et al. have studied extensively the sorption of $Cu^{2+}$ and $Pb^{2+}$ onto other metal-oxide nanomaterials. For instance, the sorption of both $Cu^{2+}$ and $Pb^{2+}$ with ZnO were pH independent over the pH's range tested; however, the sorption of both ions with $Fe_3O_4$ and CuO increased as the pH of the solution increased (Mahdavi et al. 2012). In another study, (Mahdavi et al. 2013) showed that the sorption of both $Cu^{2+}$ and $Pb^{2+}$ onto MgO was pH independent and remained unaffected as the pH of the solutions increased, while with $Al_2O_3$ and $TiO_2$, the binding increased as a function of pH from 2 to 7 (Cantu et al. 2018). Cantu et al. showed that the binding of $Cu^{2+}$with $Fe_7S_8$ was pH independent between pH 2–6 while the binding of $Pb^{2+}$ increased as pH was increased. Similarly, Zepeda et al. (2018) showed that the sorption of $Cu^{2+}$ onto $SnO_2$ increased as the pH of the solution increased with an optimal pH of 5. Ammar et al. investigated $CaSiO_3$/CuO composite nanoparticles for cadmium removal, which expressed a maximum binding at pH 9. The pH dependence on metal adsorption was determined to be a competition of $Cd^{2+}$ and $CdOH^+$ (Ammar et al. 2017). The binding of metal ions has been linked to the surface chemistry which includes the pKa of surface groups and the point of zero charge (PZC) (Wang et al. 2011). The pKa for ZnS has not been determined experimentally. However, for zinc sulfide, the PZC has been determined to be approximately at pH 2.5 (Wang et al. 2011). Above pH 2.5, the surface of ZnS nanoparticles becomes negatively charged and attractive to metal ions such as $Cu^{2+}$ and $Pb^{2+}$, which is consistent with the pH profiles observed in the present study, where an increase in binding was observed with increasing pH. The PZC should be in the point at which deprotonation of the surface begins where one could assume the pKa of the ZnS should be around pH 2.5. The PZC change should be in the pH region, where binding begins to increase would indicate that there is an electrostatic attraction of the metal ion to the ZnS nanoparticles. The attraction of the metal ion is followed by the formation of either Cu–S or Pb–S bond and eventually leads to the formation of the crystalline sulfide phase.

## Time dependence and sorption kinetics

Figure 5a, b, and c shows the results from the time dependence study for the sorption of $Cu^{2+}$ under ambient light, $Pb^{2+}$ under ambient light, and $Pb^{2+}$ under dark conditions onto the ZnS nanoparticles at temperatures of 4, 22, and 45 °C. Under ambient light conditions, it was determined that the sorption of both ions occurred within the first 5 min of contact with ZnS and did not change dramatically thereafter (Fig. 5A). Furthermore, increasing the temperature had no impact on the binding of either ion onto ZnS under ambient light conditions (Fig. 5b). Similar results have been observed in other

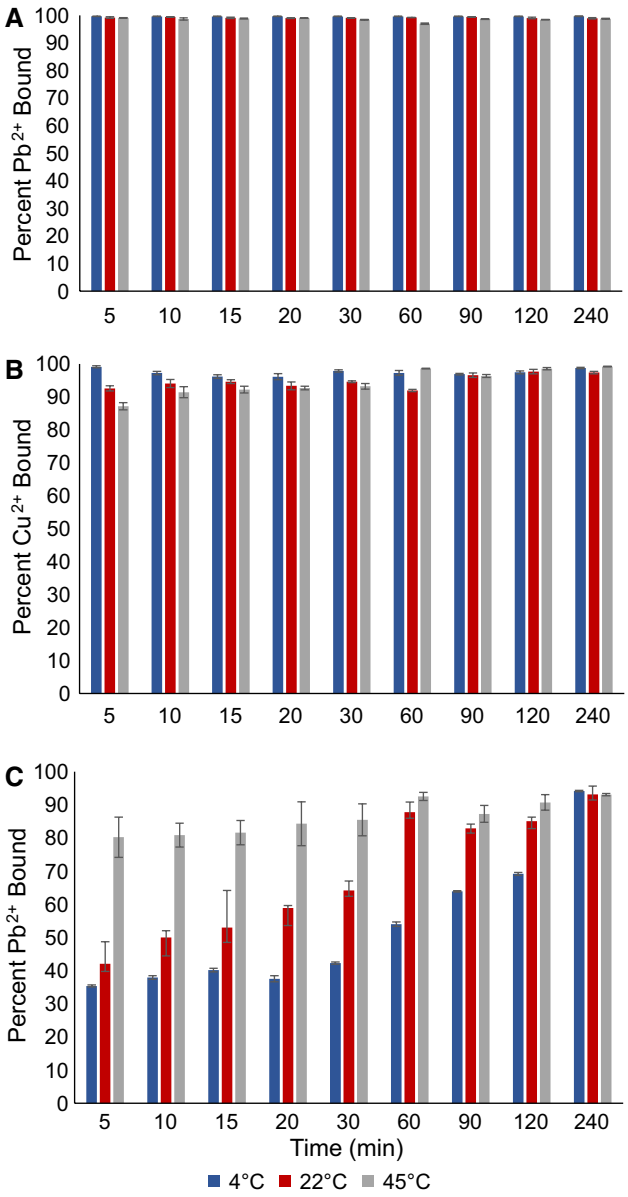


**Fig. 5** Time dependence study for the adsorption of $Pb^{2+}$ (**a**) $Cu^{2+}$ with ZnS under ambient lighting (**b**) and the reaction with $Pb^{2+}$ under dark conditions (**c**) at temperature of 4, 22 and 45 °C

adsorption studies between metal sulfides and metal oxides and dissolved metal ions (Tamez et al. 2016; Valle et al. 2017). Since the sorption occurred within the first 5 min, neither a kinetics model or an Arrhenius plot could have been constructed. However, both time and temperature did affect the $Pb^{2+}$ binding to the ZnS under dark conditions as shown in Fig. 5c. The kinetics data for the $Pb^{2+}$ binding to the ZnS under dark conditions were extracted and fitted and was determined that the sorption followed zeroth-order kinetics, as defined in Eq. 2:

$$-\frac{d[Pb]}{dt} = k[Pb]^0 \tag{2}$$

where d[Pb] is the change of lead concentration, dt is the change in time, k is the rate constant. The zero-order kinetics model defined that there was a direct relationship between the change in concentration and the change in time. In the present study, the rate of removal was followed and thus a positive rate constant was determined. A zeroth-order kinetics model has been observed in many adsorption studies (Cantu et al. 2018; Luther et al. 2013; Rajurkar et al. 2011; Zepeda et al. 2018). As can be seen in Fig. 6A, the rate of the reaction directly varied with the change in temperature, the rate constant at the highest temperature was 0.631 ppm/min while the rate constant at the lowest temperature was 0.256 ppm/min. The reaction times changed according to the temperature, at 45 °C the reactions took 30 min to complete, at 25 °C the reaction took 90 min to complete while the samples at 4 °C took 240 min to complete. Ammar et al. using $CaSiO_3$/CuO composite nanoparticles determined time for cadmium to completely bind from a 25 ppm solution required 60 min [Ammar et al. 2017].

The activation energy of the reaction was determined based on the values of the rate constants determined from the zero-order kinetics. Using the rate constants from the reactions at the three temperatures, an Arrhenius plot was developed with the line defined by the Arrhenius equation (Eq. 3):

$$\ln(k) = -\frac{E_a}{RT} - \ln(A) \tag{3}$$

where the ln(k) is the natural log of the rate constant, $E_a$ is the activation energy (J/mol), R is the gas constant (8.314 J/mol K), T is the temperature in K, and ln(A) is the frequency pre-factor of the reaction. By plotting ln(k) versus 1/T, the slope of the line is defined as the activation energy (divided by R) while the y intercept is the frequency pre-factor. The Arrhenius plot for the binding of the $Pb^{2+}$ ions to the ZnS nanoparticles under dark conditions is shown in Fig. 6B. The activation energy for the reaction was determined to be 16.3 kJ/mol. According to previous studies, the magnitude of the activation energy can be used to identify the

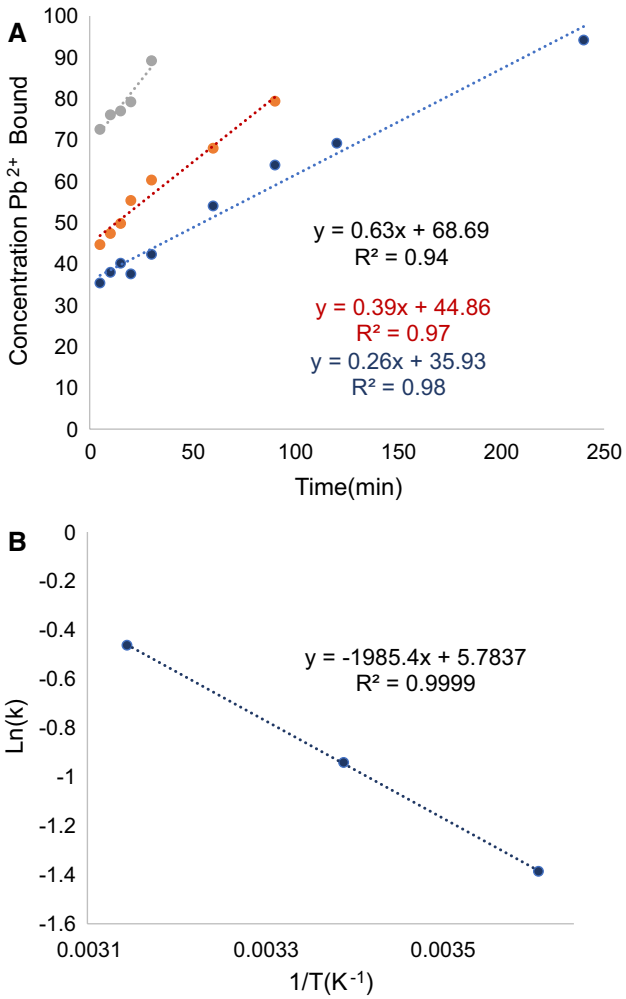


**Fig. 6** Kinetics plot for the binding of $Pb^{2+}$ under dark conditions at temperature of 4, 22, and 45° (**a**). Arrhenius plot for binding of $Pb^{2+}$ to ZnS under dark conditions (**b**)

type of adsorption occurring between the nano-sorbent and the ionic species. Energies ranging between 40 and 80 kJ/mol indicated a chemisorption process while energies below 40 kJ/mol indicated a physisorption process (Boparai et al. 2011; Cantu et al. 2014; Mahmood et al. 2011). Based on the calculated activation energy for the binding in the present study, the sorption process occurring between $Pb^{2+}$ and ZnS in the dark was physisorption, which has been observed for the interaction of metal ions with different sorbents (Boparai et al. 2011; Cantu et al. 2014; Mahmood et al. 2011).

## Isotherms

Table 5 shows the capacities determined for the binding of $Cu^{2+}$ and $Pb^{2+}$ to ZnS in both ambient light and the $Pb^{2+}$ binding under dark conditions. The sorption processes for both ions onto the nano-sorbent in light conditions and the

**Table 5** Adsorption capacities for the binding of $Cu^{2+}$ and $Pb^{2+}$ with ZnS nano-sorbent following the Langmuir isotherm model

| Light condition | Ion | T (K) | Capacity (mg/g) | Capacity (mmol/g) |
|---|---|---|---|---|
| Ambient light | $Cu^{2+}$ | 277 | 116.3 | 1.83 |
| | | 295 | 212.8 | 3.35 |
| | | 318 | 243.9 | 3.84 |
| | $Pb^{2+}$ | 277 | 39.1 | 0.189 |
| | | 295 | 128.2 | 0.619 |
| | | 318 | 147.1 | 0.710 |
| Dark | $Pb^{2+}$ | 277 | 36.1 | 0.174 |
| | | 295 | 54.1 | 0.261 |
| | | 318 | 79.4 | 0.383 |

$Pb^{2+}$ under the dark conditions were determined to follow the Langmuir isotherm model (Eq. 4):

$$\frac{1}{q_e} = \frac{1}{q_m} + \frac{1}{K_a q_m C_e} \tag{4}$$

where the removal capacity at any concentration is defined as $q_e$, the maximum binding capacity as $q_m$, the equilibrium concentration as $C_e$, and an equilibrium constant as $K_a$.

As shown in Table 5, the binding capacity of the ZnS in ambient light for both $Cu^{2+}$ and $Pb^{2+}$ increases as a function of temperature from 4 to 45 °C. At all three temperatures investigated in this work, $Cu^{2+}$ (1.8–3.84 mmol/g) bound more to ZnS in ambient light than $Pb^{2+}$ (0.189–0.710 mmol/g), indicating that $Cu^{2+}$ binds in higher concentrations compared to the $Pb^{2+}$. An increase in binding capacity with increasing temperature is indicative of an endothermic reaction occurring for both ions. Similarly, the sorption of $Pb^{2+}$ with ZnS (dark), shown in Table 5, also increased as a function of temperature from 4 to 45 °C, which indicated an endothermic reaction. The $Pb^{2+}$ binding under the dark reaction conditions was lower than the observed binding in the ambient light conditions at the highest temperature. The data indicated there was an impairment for the binding in the absence of light. The light may have contributed to the formation of PbS, which was shown in the diffraction data as a reaction product between the $Pb^{2+}$ and ZnS. The formation of PbS after reaction with a transition metal-sulfide nanomaterial has been shown after the reaction of $Pb^{2+}$ with $TiS_2$ nanoparticles (Cantu et al. 2019).

Recent studies on the sorption of $Pb^{2+}$ and $Cu^{2+}$ with nano-sorbents showed inconsistent results which can be observed in Table 6 (Cantu et al. 2019; Castaldi et al. 2015; Chen and Li 2010; Gao et al. 2009; Hua et al. 2012; Lee et al. 2015; Mahdavi et al. 2012, 2013, 2007; Nadaroglu et al. 2010; Sitko et al. 2013; Tamez et al. 2016; Wang et al. 2006; Wu et al. 2013; Zepeda et al. 2018). For instance, Fe–water residues also exhibited low capacities of 6.7 mg/g and 40.8 mg/g for the sorption of $Cu^{2+}$ and $Pb^{2+}$ (Castaldi et al. 2015). Additionally, the use of graphene oxide for the sorption of $Zn^{2+}$, $Cd^{2+}$, $Pb^{2+}$, and $Cu^{2+}$ has shown capacities of 345, 530, 1119, and 294 mg/g, respectively (Sitko et al. 2013). Cobalt-modified ferrite nanoparticles have shown $Cu^{2+}$ binding capacities of 164.2 mg/g (2.6 mmol/g) (Vamvakidis et al. 2020). $TiO_2$ on the other hand, has shown relatively low capacities of 21.7 and 50.2 mg/g for $Pb^{2+}$ and $Cu^{2+}$, respectively (Mahdavi et al. 2013). Shahrashoub et al. showed active carbon carbon/magnetite composite materials had low binding capacity of 13.37 mg/g or approximately 0.21 mmol/g for $Cu^{2+}$ ions (Shahrashoub et al. 2021). Similarly, Cantu et al. showed low capacities of 8.09 mg/g and 5.29 mg/g for the sorption of $Pb^{2+}$ and $Cu^{2+}$ with $Fe_7S_8$, respectively, at room temperature (Cantu et al. 2018). In another study, Cantu et al. reported a binding capacity of 0.80 mMol/g (165.6 mg/g) and 3.50 mMol/g (222.4 mg/g) for $Pb^{2+}$ and $Cu^{2+}$ binding to $TiS_2$ nanoparticles at room temperature, respectively (Cantu et al. 2019). In addition, Wang et al. have investigated the binding of $Pb^{2+}$ to disulfide cross-linked poly(methacrylic acid) iron oxide nanoparticles which had a binding capacity of approximately 49 mg/g (0.24 mmol/g) (Wang et al. 2021), whereas Qu et al. studied the binding of $Pb^{2+}$ to activated carbon-supported sulfide nZVI which had a binding capacity of 295.30 mg/g (1.45 mmol/g) (Qui et al. 2021).

Thermodynamics of the binding were determined based on the isotherm study performed at different temperatures. From the data, the enthalpy, entropy, and Gibbs free energy for the reactions of $Cu^{2+}$ and $Pb^{2+}$ with ZnS under ambient light and the $Pb^{2+}$ binding under dark conditions were determined. The results of the thermodynamics for the binding are presented in Table 7. The ΔG was determined using Eq. 5, which shows the relationship between ΔG and the distribution coefficients for the reactions between the ZnS nano-sorbent and the ions.

$$\Delta G = -RT\ln(K_d). \tag{5}$$

ΔG is the change in Gibbs free energy; R is the gas constant (8.314 J/mol K); T is temperature in K; and $K_d$ is the distribution coefficients. Table 7 shows the thermodynamic parameters for adsorption of both $Cu^{2+}$ and $Pb^{2+}$. As can be seen in Table 7, the sorption process for the $Pb^{2+}$ ions under ambient light conditions was spontaneous at all temperatures tested, as indicated by the negative ΔG values. However, the $Cu^{2+}$ binding was non-spontaneous at the three temperatures tested, but the binding did become more spontaneous as the temperature was increased as indicated by the decreasing ΔG values as the temperature increased. For instance, the ΔG value for the sorption of $Cu^{2+}$ at 4 °C was 6.89 kJ/mol and decreased to 4.84 kJ/mol at 45 °C. The ΔG value for the sorption of $Pb^{2+}$ at 4 °C was − 4.93 kJ/mol and decreased to -9.98 kJ/mol at 45 °C. Similarly, the sorption of $Pb^{2+}$ in dark conditions increased

**Table 6** Binding capacities of reported nano-sorbents for the removal of $Cu^{2+}$ and $Pb^{2+}$ in aqueous solutions

| Ion | Material | Capacity (mmol/g) | Capacity (mg/g) | References |
|---|---|---|---|---|
| $Cu^{2+}$ | Graphene oxide | 1.84 | 117.5 | (Wu et al. 2013) |
| | $Fe_2O_3$ | 0.23 | 19.61 | (Tamez et al. 2016) |
| | $Fe_3O_4$ | 0.81 | 37.04 | (Tamez et al. 2016) |
| | $TiO_2$ | 0.79 | 50.2 | (Mahdavi et al. 2013) |
| | $Al_2O_3$ | 0.754 | 47.9 | (Mahdavi et al. 2013) |
| | MgO | 2.45 | 149.1 | (Mahdavi et al. 2013) |
| | ZnO | 0.54 | 137.5 | (Mahdavi et al. 2012) |
| | CuO | 0.19 | 54.1 | (Mahdavi et al. 2012) |
| | $Fe_3O_4$ | 0.49 | 14.7 | (Mahdavi et al. 2012) |
| | $SnO_2$ | 0.046 | 2.95 | (Zepeda et al. 2018) |
| | Graphene oxide | 4.63 | 294 | (Sitko et al. 2013) |
| | $Fe_7S_8$ | 0.102 | 5.29 | (Cantu et al. 2018) |
| | Fe-WTR | 0.106 | 6.7 | (Castaldi et al. 2015) |
| | Al-WTR | 0.073 | 4.64 | (Castaldi et al. 2015) |
| | Red mud | 0.084 | 5.35 | (Nadaroglu et al. 2010) |
| | $CeO_2$ | 0.044 | 15.4 | (Hua et al. 2012) |
| | Fe(OOH) (goethite) | 2.350 | 149.25 | (Chen and Li, 2010) |
| | Coal ash | 0.661 | 42.0 | (Wang et al. 2006) |
| | $Mn_3O_4$ | 0.020 | 1.24 | (Lee et al. 2015) |
| | Activated Carbon (AC) | 0.094 | 6.09 | (Lee et al. 2015) |
| | $Mn_3O_4$/AC | 0.583 | 37.04 | (Lee et al. 2015) |
| | Oxidized carbon nanotubes | 0.040 | 2.57 | (Gao et al. 2009) |
| | $TiS_2$ nanoparticles | 3.50 | 222.4 | (Cantu et al. 2019) |
| | Cobalt ferrite | 2.6 | 164.2 | (Vamvakidis et al. 2020) |
| | Carbon Magnetite | 0.21 | 13.37 | (Shahrashoub et al. 2021) |
| | $Fe_2O_3$ | 0.31 | 47.62 | (Tamez et al. 2016) |
| | $Fe_3O_4$ | 0.58 | 166.67 | (Tamez et al. 2016) |
| | $TiO_2$ | 0.105 | 21.7 | (Mahdavi et al. 2013) |
| | $Al_2O_3$ | 0.199 | 41.2 | (Mahdavi et al. 2013) |
| | MgO | 0.717 | 148.6 | (Mahdavi et al. 2013) |
| | ZnO | 2.16 | 112.7 | (Mahdavi et al. 2012) |
| | CuO | 0.85 | 39.4 | (Mahdavi et al. 2012) |
| | $Fe_3O_4$ | 0.23 | 101.4 | (Mahdavi et al. 2012) |
| | Graphene oxide | 5.40 | 1119 | (Sitko et al. 2013) |
| $Pb^{2+}$ | $Fe_7S_8$ | 0.039 | 8.09 | (Cantu et al. 2018) |
| | Fe-WTR | 0.194 | 40.8 | (Castaldi et al. 2015) |
| | Al-WTR | 0.065 | 13.47 | (Castaldi et al. 2015) |
| | $CeO_2$ | 0.240 | 9.2 | (Hua et al. 2012) |
| | $MnO_2$/CNTs | 0.380 | 78.74 | (Wang et al. 2007) |
| | $Mn_3O_4$ | 0.037 | 7.57 | (Lee et al. 2015) |
| | Activated Carbon (AC) | 0.131 | 27.17 | (Lee et al. 2015) |
| | $Mn_3O_4$/AC | 0.287 | 59.52 | (Lee et al. 2015) |
| | $TiS_2$ nanoparticles | 0.80 | 165.6 | (Cantu et al. 2019) |
| | Poly(methacrylic acid) iron oxide nanoparticles | 0.24 | 49.0 mg/g | (Wang et al. 2021) |
| | Activated carbon-supported sulfide nZVI | 1.45 | 295.0 mg/g | (Qui et al. 2021) |

**Table 7** Thermodynamic parameters for the sorption of $Cu^{2+}$ and $Pb^{2+}$ with the ZnS nano-sorbent in different light conditions

| Light condition | Ion | T (K) | ΔG (kJ/mol) | ΔH (kJ/mol) | ΔS (J/mol) |
|---|---|---|---|---|---|
| Ambient light | $Cu^{2+}$ | 277 | 6.39 | 16.84 | 37.91 |
| | | 298 | 5.73 | | |
| | | 315 | 4.84 | | |
| | $Pb^{2+}$ | 277 | −2.67 | 16.08 | 66.51 |
| | | 298 | −3.48 | | |
| | | 318 | −5.42 | | |
| Dark | $Pb^{2+}$ | 277 | −1.22 | 13.79 | 54.01 |
| | | 298 | −2.46 | | |
| | | 318 | −3.43 | | |

spontaneously as a function of temperature where at 4 °C, the ΔG was − 2.81 kJ/mol and decreased to − 5.56 kJ/mol at 45 °C. Ben-Ali et al. showed that the use of pomegranate peel for the binding of $Cu^{2+}$ was spontaneous at high temperatures with ΔG values of − 5.36 and − 7.41 kJ/mol for 303 K and 313 K, respectively (Ben-Ali et al. 2017). The use of ZnO nanorods for the sorption of $Pb^{2+}$ was spontaneous at all temperatures tested with ΔG values ranging from − 8.41 to − 10.07 kJ/mol for 303 K to 323 K (Kumar et al. 2013). Additionally, Rafiq et al. showed that the sorption of $Cu^{2+}$ onto MgO had ΔG values ranging from -0.35 to -3.26 kJ/mol over a temperature range between 323 and 343 K, indicating that the sorption was near equilibrium and spontaneous (Rafiq et al. 2014). The sorption of $Cu^{2+}$ and $Pb^{2+}$ with manganese oxide coated on zeolite was spontaneous at temperatures of 288, 303, and 313 K with ΔG values ranging from − 50.5 to − 56.5 kJ/mol for $Cu^{2+}$ and − 50.5 to − 56.7 kJ/mol for $Pb^{2+}$ (Zou et al. 2006). Moreover, Cantu et al. showed that the sorption of both $Cu^{2+}$ and $Pb^{2+}$ onto $Fe_7S_8$ was non-spontaneous at low temperatures with ΔG values of 9.78 and 4.60 kJ/mol for $Cu^{2+}$ and 5.07 and 1.44 kJ/mol for $Pb^{2+}$ for temperatures of 277 and 295 K, respectively (Cantu et al. 2018). However, at a temperature of 318 K, the sorption of both $Cu^{2+}$ and $Pb^{2+}$ was spontaneous with ΔG values of − 11.23 and − 2.45 kJ/mol, respectively (Cantu et al. 2018).

Figure 7a and b shows the thermodynamics plots determined from the isotherm studies which were obtained from plotting ln $K_d$ vs 1/T ($K^{-1}$). Figure 7a shows the binding for both the $Cu^{2+}$ and $Pb^{2+}$ ions to the ZnS nanoparticles under ambient light conditions. Figure 7b shows the thermodynamics plot for the binding of $Pb^{2+}$ ions to the ZnS under the dark conditions. From the thermodynamics plots, the fitting of the line was used to determine the $\Delta H$ and $\Delta S$ values for the sorption process of both ions. The relationship between ln $K_d$, $\Delta H$, and $\Delta S$ is given in Eq. 6:

$$\ln\left(K_d\right) = \frac{\Delta S}{R} - \frac{\Delta H}{RT} \quad (6)$$

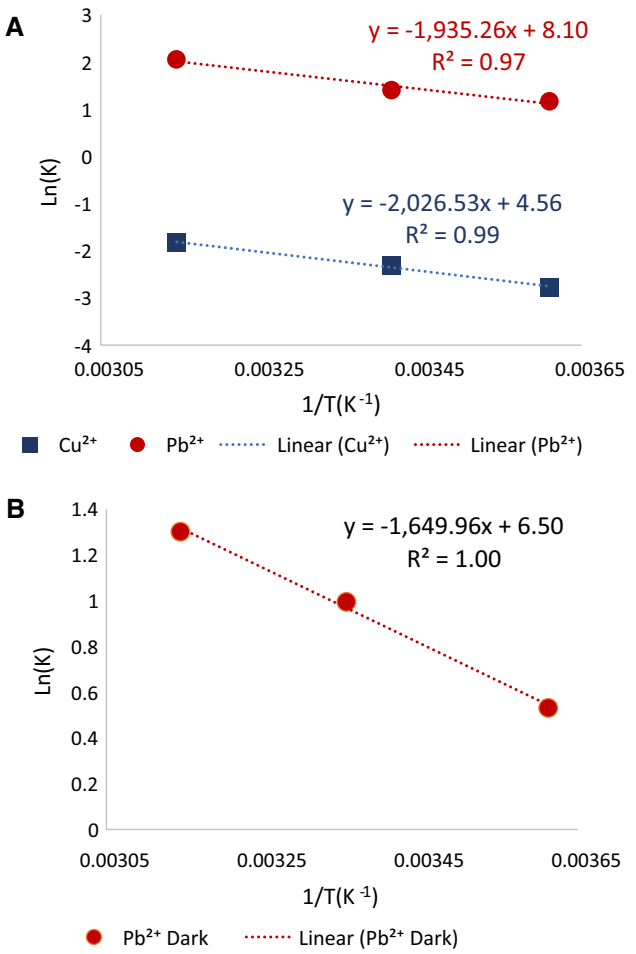


**Fig. 7** Thermodynamics plots for the binding of $Cu^{2+}$ and/or $Pb^{2+}$ with ZnS under ambient lighting (**a**) and dark conditions (**b**)

where $K_d$ is the distribution coefficient; $\Delta S$ is the change in entropy; R is the gas constant (8.314 J/mol K); T is the temperature in Kelvin; and ΔH is the change in enthalpy. The $\Delta S$ value was determined from the y intercept of the line while the ΔH value was determined from the slope of the line. As illustrated in Table 7, the ΔH values for the sorption of $Cu^{2+}$ and $Pb^{2+}$ to ZnS in ambient light were 16.84 and 16.08 kJ/mol, respectively, indicating an endothermic reaction occurs. Correspondingly, the binding of $Pb^{2+}$ with ZnS under dark conditions was determined to be 13.79 kJ/mol, which was attributed to an endothermic process occurring during adsorption. Similarly, other studies have shown adsorption of metal ions onto metal oxides/sulfides occur via endothermic processes (Cantu et al. 2018; Zepeda et al. 2018). Based on the magnitude of the ΔH, the sorption of both ions in ambient light occurred via physisorption. Furthermore, the sorption of $Pb^{2+}$ with ZnS in dark conditions occurred through an ion exchange mechanism almost at the energy of a physisorption process. Based on literature data, adsorption reactions consisting of ΔH below 40 kJ/

mol corresponded to physisorption while ΔH values ranging between 8 and 16 kJ/mol indicated an ion exchange process (Al-Anber 2011; Cantu et al. 2018; Luther et al. 2013).

## Interference study

The results for the interference study are shown in Figs. 7 and 8 for the sorption of $Pb^{2+}$ and $Cu^{2+}$ with ZnS in both ambient light and the sorption of $Pb^{2+}$ ion under the dark conditions in the presence of individual and combination cationic interferences. The cationic interference ions used for each study were $Na^+$, $Mg^{2+}$, $K^+$, and $Ca^{2+}$, which are commonly found in natural waters, with increasing concentrations from 0.3 to 1000 ppm while the concentrations of $Cu^{2+}$ and $Pb^{2+}$ were held constant at 0.3 ppm. Figure 8a shows the binding of $Pb^{2+}$ with ZnS in ambient light in the presence of all cations. As seen in Fig. 8a, the presence of each individual cation with increasing concentration had little to no effect on the sorption of $Pb^{2+}$ in ambient lighting. The sorption of $Pb^{2+}$ in the presence of a combination of all cations investigated showed a slight increase in binding as a function of concentration. For example, in the presence of 0.3 ppm of cations, the binding was approximately 88%. The sorption then increased steadily to 100% binding at 300 ppm of the cations and remained constant thereafter. Similarly, as seen in Fig. 8B, the sorption of $Pb^{2+}$ under the dark conditions using the same cations showed to have a synergistic effect as a function of increasing concentration. The binding of $Pb^{2+}$ in the presence of all cations in dark conditions had the same trend as the sorption of $Pb^{2+}$ in ambient light, which showed a slight increase with increasing concentration of interferences. However, the sorption of $Cu^{2+}$ in the presence of the divalent cations was observed to decrease as the concentration of the cations increased (Fig. 8c). In fact, $Na^+$ and $K^+$ caused an antagonistic effect at concentrations above 100 ppm. As can be seen in Fig. 8c, the sorption of $Cu^{2+}$ in the presence of sodium was 100% binding from 0.3 to 100 ppm $Na^+$, but from 300 to 1000 ppm $Na^+$, the binding of $Cu^{2+}$ decreased slightly to approximately 90%. The presence of all cations in the sorption of $Cu^{2+}$ with ZnS in ambient light was observed to decrease with increasing concentration of interferences. As can be seen in Fig. 8c, the sorption of $Cu^{2+}$ in the presence of 0.3 ppm cations was 100% and it decreased thereafter to approximately 35% in the presence of 1000 ppm of all cations.

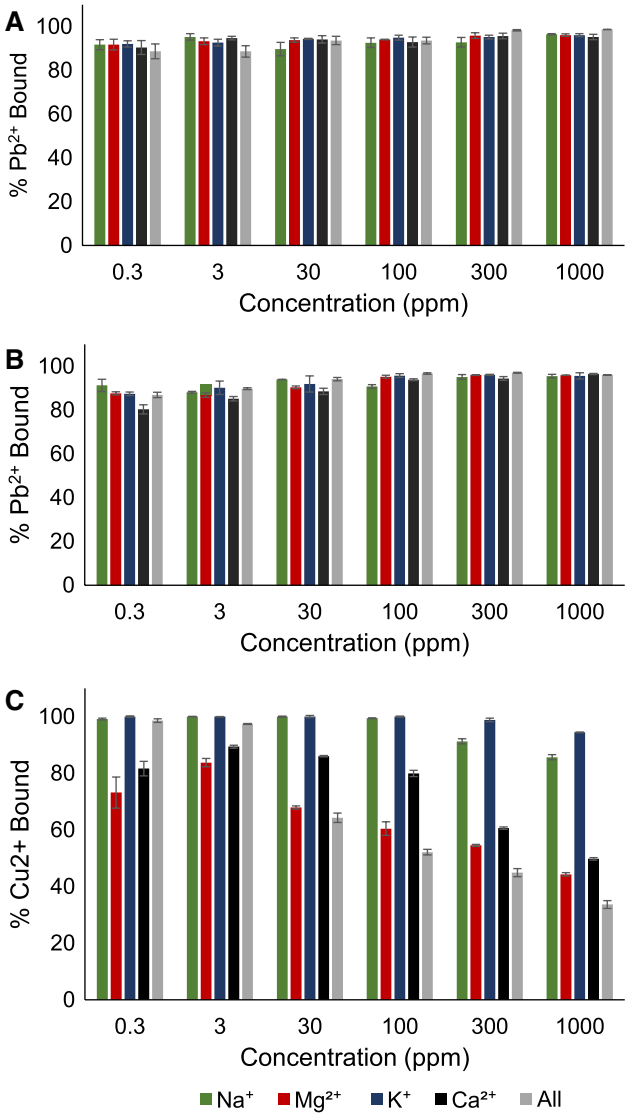


**Fig. 8** Binding of $Pb^{2+}$ with ZnS coexisting with cationic interfering species under ambient light (**a**), dark conditions (**b**), and binding of $Cu^{2+}$ with ZnS nanoparticles with cationic interfering species under ambient light (**c**)

A study performed by Tamez et al. showed that the presence of $Na^+$, $Mg^{2+}$, $K^+$, or $Ca^{2+}$ had no effect on the sorption of $Pb^{2+}$ with $Fe_3O_4$ (Tamez et al. 2016). However, in the presence of $Na^+$ or $Ca^{2+}$, a synergistic effect on the binding of $Pb^{2+}$ with $Fe_2O_3$ was reported (Tamez et al. 2016). Similarly, Cantu et al. showed that the sorption of $Pb^{2+}$ with $Fe_7S_8$ in the presence of $Na^+$, $Mg^{2+}$, $K^+$, and $Ca^{2+}$ had no effect on the sorption (Cantu et al. 2018). Moreover, $Cu^{2+}$ sorption with $Fe_7S_8$ in the presence of any of the cations showed an antagonistic effect as a function of concentration (Cantu et al. 2018). The decrease in the $Cu^{2+}$ binding with increasing concentration of interfering ion may be a function of the cation and counter ions affecting the copper interaction with the sulfur ions on the surface. Ejtemaei and Nguyen have shown that $Ca^{2+}$ and $Mg^{2+}$ ions can decrease the binding of $Cu^{2+}$ and the hydrophobicity of sphalerite (Ejtemaei and Nguyen 2017). However, the authors did not observe any major binding of $Ca^{2+}$ or $Mg^{2+}$ to the surface of the sphalerite, but copper binding was reduced as well as the formation of CuS. The results indicated that $Ca^{2+}$ and $Mg^{2+}$ do compete with the surface sites for $Cu^{2+}$ binding. In the

present study, the metal sulfide showed a preferential binding to both the $Cu^{2+}$ and $Pb^{2+}$ over the hard cation interferences. The preference in the binding is more than likely due to the solubility of the CuS and PbS formed during the binding process. PbS and CuS have solubility products of $1.6\times10^{-29}$ and $4.07\times10^{-22}$, respectively (Lawrence and Johnston 1980; Huang et al. 2009), whereas the alkali metals and alkali earth metals are soluble or decompose in water, which results in lower stability and lower interference on the binding even at very high concentration ratios of interference to $Cu^{2+}$ or $Pb^{2+}$ ion. In the combined interference study, there was a mg /L ratio of 13,333:1 mg interference: mg $Cu^{2+}$ or $Pb^{2+}$ ratio and still the heavy metals bound to the ZnS.

## Conclusion

The ZnS nano-sorbent was successfully synthesized using a hydrothermal method and was determined to be in a cubic lattice with an average crystallite size of 7 nm using XRD analysis. The binding of $Cu^{2+}$ was slightly pH dependent and increased as a function of pH while $Pb^{2+}$ was pH independent under ambient light. The use of UV light had little to no effect on the binding of either $Cu^{2+}$ or $Pb^{2+}$ ions. However, the absence of light (i.e., reactions performed in the dark) showed a decrease for the binding of $Pb^{2+}$. The binding of both $Pb^{2+}$ and $Cu^{2+}$ to ZnS in ambient light was time independent after the first 5 min of equilibration. The binding of $Pb^{2+}$ in dark conditions increased as a function of time and was determined to follow the zero-order kinetics model while the rate increased with increasing temperature indicating an endothermic reaction. The binding of $Pb^{2+}$ under ambient light and dark conditions was spontaneous at all temperatures tested and increased in spontaneity as a function of increasing temperature. While the binding of $Cu^{2+}$ under ambient light was found to be close to equilibrium, the $\Delta G$ value was positive. The magnitude of the $\Delta H$ value indicated that the sorption of both $Pb^{2+}$ and $Cu^{2+}$ in ambient light and $Pb^{2+}$ in the dark occurred through physisorption. Finally, the presence of interfering cations showed little to no effect on the sorption of $Pb^{2+}$ under either ambient light or no light conditions while the sorption of $Cu^{2+}$ was observed to decrease as the concentrations of interfering cations increased. Although the binding was suppressed slightly, the results showed preferential binding of the $Cu^{2+}$ and $Pb^{2+}$ ion to the ZnS nanomaterial. In the combined interference study, there was mg /L ratio of 13,333:1 mg interference: mg $Cu^{2+}$ or $Pb^{2+}$ ratio and still the heavy metals bound to the ZnS.

**Acknowledgements** The Department of Chemistry at the University of Texas Rio Grande Valley is grateful for the generous support provided by a Departmental Grant from the Robert A. Welch Foundation (Grant No. BX-0048). This work was the funding support received by NSF PREM award under grant No. DMR-2122178: UTRGV-UMN Partnership for Fostering Innovation by Bridging Excellence in Research and Student Success.

**Authors' contribution** All authors contributed to the study conception and design. Material preparation, data collection, and analysis were performed by JMC, JPV, AP, CV, KF, HMM, EF, MA, EK, and JGP. The first draft of the manuscript was written by J.M. Cantu, and all authors commented on previous versions of the manuscript. All authors read and approved the final manuscript.

**Funding** Finiancial support was obtained from a Departmental Grant from the Robert A. Welch Foundation Grant No. BX-0048). In addition, this work was also funded by NSF PREM (DMR-2122178): UTRGV-UMN Partnership for Fostering Innovation by Bridging Excellence in Research and Student Success.

## Declarations

**Conflict of interest** The authors declare that they have no conflict of interest.

**Availability of data and materials** Data are available upon request.

**Code availability** No code was used.

## References

Ahmad A, Rafatullah M, Sulaiman O, Ibrahim MH, Chii YY, Siddique BM (2009) Removal of Cu(II) and Pb(II) ions from aqueous solutions by adsorption on sawdust of Meranti wood. Desalination 247:636–646. https://doi.org/10.1016/j.desal.2009.01.007

Al-Anber MA (2011) Thermodynamics approach in the adsorption of heavy metals, in: Thermodynamics - Interaction Studies - Solids, Liquids and Gases. InTech. https://doi.org/10.5772/21326

Alghamdi AA, Al-Odayni A-B, Saeed WS, Al-Kahtani A, Alharthi FA, Aouak T (2019) Efficient adsorption of lead (II) from aqueous phase solutions using polypyrrole-based activated carbon. Materials (Basel) 12:2020. https://doi.org/10.3390/ma12122020

Ammar N, Youssef AFA, Kenawy SH, Hamzawy EMA, El-Khateeb MA (2017) Wollastonite ceramic/CuO nano-composite for cadmium ions removal from waste water. Egypt J Chem 60:817–823

Anthemidis AN, Ioannou K-IG (2009) Recent developments in homogeneous and dispersive liquid–liquid extraction for inorganic elements determination: a review. Talanta 80:413–421. https://doi.org/10.1016/j.talanta.2009.09.005

Azzam AM, El-Wakeel ST, Mostafa BB, El-Shahat MF (2016) Removal of Pb, Cd, Cu and Ni from aqueous solution using nano scale zero valent iron particles. J Environ Chem Eng 4:2196–2206. https://doi.org/10.1016/j.jece.2016.03.048

Barlokova D, Ilavsky J, Marton M, Kunstek M (2019) Removal of heavy metals in drinking water by iron-based sorption materials. IOP Conf Ser Earth Environ Sci 362, 012109. https://doi.org/10.1088/1755-1315/362/1/012109

Ben-Ali S, Jaouali I, Souissi-Najar S, Ouederni A (2017) Characterization and adsorption capacity of raw pomegranate peel biosorbent for copper removal. J Clean Prod 142:3809–3821. https://doi.org/10.1016/j.jclepro.2016.10.081

Berry LG (1954) The crystal structure of covellite, CuS and klockmannite. CuSe Am Miner 39:504–509

Boparai HK, Joseph M, O'Carroll DM (2011) Kinetics and thermodynamics of cadmium ion removal by adsorption onto nano zerovalent iron particles. J Hazard Mater 186:458–465. https://doi.org/10.1016/j.jhazmat.2010.11.029

Cantu Y, Remes A, Reyna A, Martinez D, Villarreal J, Ramos H, Trevino S, Tamez C, Martinez A, Eubanks T, Parsons JG (2014) Thermodynamics, kinetics, and activation energy studies of the sorption of chromium(III) and chromium(VI) to a $Mn_3O_4$ nanomaterial. Chem Eng J 254:374–383. https://doi.org/10.1016/j.cej.2014.05.110

Cantu J, Gonzalez DF, Cantu Y, Eubanks TM, Parsons JG (2018) Thermodynamic and kinetic study of the removal of $Cu^{2+}$and $Pb^{2+}$ions from aqueous solution using $Fe_7S_8$ nanomaterial. Microchem J. https://doi.org/10.1016/j.microc.2018.04.003

Cantu J, Valle J, Flores K, Gonzalez D, Valdes C, Lopez J, Padilla V, Alcoutlabi M, Parsons J (2019) Investigation into the thermodynamics and kinetics of the binding of $Cu^{2+}$ and $Pb^{2+}$ to $TiS^2$ nanoparticles synthesized using a solvothermal process. J Environ Chem Eng. https://doi.org/10.1016/j.jece.2019.103463

Castaldi P, Silvetti M, Garau G, Demurtas D, Deiana S (2015) Copper(II) and lead(II) removal from aqueous solution by water treatment residues. J Hazard Mater 283:140–147. https://doi.org/10.1016/j.jhazmat.2014.09.019

Chen YH, Li FA (2010) Kinetic study on removal of copper(II) using goethite and hematite nano-photocatalysts. J Colloid Interface Sci 347:277–281. https://doi.org/10.1016/j.jcis.2010.03.050

Clever HL, Johnston FJ (1980) The solubility of some sparingly soluble lead salts: an evaluation of the solubility in water and aqueous electrolyte solution. J Phys Chem Ref Data 9:751–784

Ejtemaei M, Nguyen AV (2017) Characterisation of sphalerite and pyrite surfaces activated by copper sulphate. Miner Eng 100:223–232

Evans HT, Konnert JA (1976) Crystal structure refinement of covellite. Am Miner 61:996–1000

Farghali AA, Bahgat M, Enaiet Allah A, Khedr MH (2013) Adsorption of Pb(II) ions from aqueous solutions using copper oxide nanostructures. Beni-Suef Univ J Basic Appl Sci 2:61–71. https://doi.org/10.1016/j.bjbas.2013.01.001

Fouladgar M, Beheshti M, Sabzyan H (2015) Single and binary adsorption of nickel and copper from aqueous solutions by γ-alumina nanoparticles: equilibrium and kinetic modeling. J Mol Liq 211:1060–1073. https://doi.org/10.1016/j.molliq.2015.08.029

Fu F, Wang Q (2011) Removal of heavy metal ions from wastewaters: a review. J Environ Manage 92:407–418. https://doi.org/10.1016/j.jenvman.2010.11.011

Fujii S, Polprasert C, Tanaka S, Hong Lien NP, Qiu Y (2007) New POPs in the water environment: distribution, bioaccumulation and treatment of perfluorinated compounds – a review paper. J Water Supply Res Technol 56:313–326. https://doi.org/10.2166/aqua.2007.005

Gaetke LM, Chow CK (2003) Copper toxicity, oxidative stress, and antioxidant nutrients. Toxicology 189:147–163. https://doi.org/10.1016/S0300-483X(03)00159-8

Gao Z, Bandosz TJ, Zhao Z, Han M, Qiu J (2009) Investigation of factors affecting adsorption of transition metals on oxidized carbon nanotubes. J Hazard Mater 167:357–365. https://doi.org/10.1016/j.jhazmat.2009.01.050

Georgopoulos PG, Wang SW, Georgopoulos IG, Yonone-Lioy MJ, Lioy PJ (2006) Assessment of human exposure to copper: a case study using the NHEXAS database. J Expo Sci Environ Epidemiol 16:397–409. https://doi.org/10.1038/sj.jea.7500462

Harsha Vardhan K, Kumar PS, Panda RC (2020) Adsorption of copper ions from polluted water using biochar derived from waste renewable resources: static and dynamic analysis. Int J Environ Anal Chem. https://doi.org/10.1080/03067319.2020.1779245

Hoa TTQ, Vu LV, Canh TD, Long NN (2009) Preparation of ZnS nanoparticles by hydrothermal method. J Phys Conf Ser 187:012081. https://doi.org/10.1088/1742-6596/187/1/012081

Hua M, Zhang S, Pan B, Zhang W, Lv L, Zhang Q (2012) Heavy metal removal from water/wastewater by nanosized metal oxides: a review. J Hazard Mater 211–212:317–331. https://doi.org/10.1016/j.jhazmat.2011.10.016

Huang Y, Xiao H, Chen S, Wang C (2009) Preparation and characterization of CuS hollow spheres. Ceram Int 35:905–907

Kaushal A, Singh S (2017) Adsorption phenomenon and its application in removal of lead from waste water: a review. Int J Hydrol. https://doi.org/10.15406/ijh.2017.01.00008

Kiflawi I, Mardix S, Steinberger IT (1969) New families of ZnS polytypes. Acta Crystallogr Sect B Struct Crystallogr Cryst Chem 25:1581–1586. https://doi.org/10.1107/S0567740869004353

Kovacova Z, Demcak S, Balintova M (2019) Removal of copper from water solutions by adsorption on spruce sawdust. Proceedings 16:52. https://doi.org/10.3390/proceedings2019016052

Kumar KY, Muralidhara HB, Nayaka YA, Balasubramanyam J, Hanumanthappa H (2013) Hierarchically assembled mesoporous ZnO nanorods for the removal of lead and cadmium by using differential pulse anodic stripping voltammetric method. Powder Technol 239:208–216. https://doi.org/10.1016/j.powtec.2013.02.009

Lee M-E, Park JH, Chung JW, Lee C-Y, Kang S (2015) Removal of Pb and Cu ions from aqueous solution by $Mn_3O_4$-coated activated carbon. J Ind Eng Chem 21:470–475. https://doi.org/10.1016/j.jiec.2014.03.006

Li Y, Gao L, Lu Z, Wang Y, Wang Y, Wan S (2020) Enhanced removal of heavy metals from water by hydrous ferric oxide-modified biochar. ACS Omega 5:28702–28711. https://doi.org/10.1021/acsomega.0c03893

Lide DR (1994) Handbook of chemistry and physics, 75th edn. CRC Press

Liu Y, Chen L, Li Y, Wang P, Dong Y (2016) Synthesis of magnetic polyaniline/graphene oxide composites and their application in the efficient removal of Cu(II) from aqueous solutions. J Environ Chem Eng 4:825–834. https://doi.org/10.1016/j.jece.2015.12.023

Luo J, Fu K, Yu D, Hristovski KD, Westerhoff P, Crittenden JC (2021) Review of advances in engineering nanomaterial adsorbents for metal removal and recovery from water: synthesis and microstructure impacts. ACS ES&T Eng. https://doi.org/10.1021/acsestengg.0c00174

Luther S, Brogfeld N, Kim J, Parsons JG (2013) Study of the thermodynamics of chromium(III) and chromium(VI) binding to iron(II/III)oxide or magnetite or ferrite and magnanese(II) iron (III) oxide or jacobsite or manganese ferrite nanoparticles. J Colloid Interface Sci 400:97–103. https://doi.org/10.1016/j.jcis.2013.02.036

Ma Q, Wang Y, Kong J, Jia H (2016) Tunable synthesis, characterization and photocatalytic properties of various ZnS nanostructures. Ceram Int 42:2854–2860. https://doi.org/10.1016/j.ceramint.2015.11.021

Mahdavi S, Jalali M, Afkhami A (2012) Removal of heavy metals from aqueous solutions using $Fe_3O_4$, ZnO, and CuO nanoparticles. J Nanoparticle Res 14:846. https://doi.org/10.1007/s11051-012-0846-0

Mahdavi S, Jalali M, Afkhami A (2013) Heavy metals removal from aqueous solutions using $TiO_2$, MgO, and $Al_2O_3$ nanoparticles. Chem Eng Commun 200:448–470. https://doi.org/10.1080/00986445.2012.686939

Mahmood T, Saddique MT, Naeem A, Mustafa S, Zeb N, Shah KH, Waseem M (2011) Kinetic and thermodynamic study of Cd(II), Co(II) and Zn(II) adsorption from aqueous solution by NiO. Chem Eng J 171:935–940. https://doi.org/10.1016/j.cej.2011.04.043

Mardix S, Alexander E, Brafman O, Steinberger IT (1967) Polytype families in zinc sulphide crystals. Acta Crystallogr 22:808–812. https://doi.org/10.1107/S0365110X67001616

Mosayebi E, Azizian S (2016) Study of copper ion adsorption from aqueous solution with different nanostructured and microstructured zinc oxides and zinc hydroxide loaded on activated carbon cloth. J Mol Liq 214:384–389. https://doi.org/10.1016/j.molliq.2015.11.036

Nadaroglu H, Kalkan E, Demir N (2010) Removal of copper from aqueous solution using red mud. Desalination 251:90–95. https://doi.org/10.1016/j.desal.2009.09.138

Needleman H (2004) Lead poisoning. Annu Rev Med 55:209–222. https://doi.org/10.1146/annurev.med.55.091902.103653

Oftedal I (1932) Die kristallstruktur des covellins (CuS). Zeitschrift Für Krist - Cryst Mater 83:9–25. https://doi.org/10.1524/zkri.1932.83.1.9

Qu J, Liu Y, Cheng L, Jiang Z, Zhang G, Deng F, Wang L, Han W, Zhang Y (2021) Green synthesis of hydrophilic activated carbon supported sulfide nZVI for enhanced Pb(II) scavenging from water: characterization, kinetics, isotherms and mechanisms. J Hazard Mater 403:123607

Rafiq Z, Nazir R, Shah MR, Ali S (2014) Utilization of magnesium and zinc oxide nano-adsorbents as potential materials for treatment of copper electroplating industry wastewater. J Environ Chem Eng 2:642–651. https://doi.org/10.1016/j.jece.2013.11.004

Rajurkar NS, Gokarn AN, Dimya K (2011) Adsorption of chromium(III), nickel(II), and copper(II) from aqueous solution by activated alumina. Clean: Soil, Air, Water 39:767–773. https://doi.org/10.1002/clen.201000273

Rodríguez-Carvajal J (1993) Recent advances in magnetic structure determination by neutron powder diffraction. Phys B 192:55–69

Sadovnikov SI, Rempel AA (2009) Crystal structure of nanostructured PbS films at temperatures of 293–423 K. Phys Solid State 51:2375–2383. https://doi.org/10.1134/S1063783409110298

Salavati-Niasari M, Ghanbari D, Loghman-Estarki MR (2012) Star-shaped PbS nanocrystals prepared by hydrothermal process in the presence of thioglycolic acid. Polyhedron 35:149–153. https://doi.org/10.1016/j.poly.2012.01.010

Santucci RJ, Scully JR (2020) The pervasive threat of lead (Pb) in drinking water: unmasking and pursuing scientific factors that govern lead release. Proc Natl Acad Sci 117:23211–23218. https://doi.org/10.1073/pnas.1913749117

Sarma GK, Sen Gupta S, Bhattacharyya KG (2019) Nanomaterials as versatile adsorbents for heavy metal ions in water: a review. Environ Sci Pollut Res 26:6245–6278. https://doi.org/10.1007/s11356-018-04093-y

Shahabuddin S, Tashakori C, Kamboh MA, Sotoudehnia Korrani Z, Saidur R, Rashidi Nodeh H, Bidhendi ME (2018) Kinetic and equilibrium adsorption of lead from water using magnetic metformin-substituted SBA-15. Environ Sci Water Res Technol 4:549–558. https://doi.org/10.1039/C7EW00552K

Shahin SA, Mossad M, Fouad M (2019) Evaluation of copper removal efficiency using water treatment sludge. Water Sci Eng 12:37–44. https://doi.org/10.1016/j.wse.2019.04.001

Shahrashou M, Bakhtiari S (2021) The efficiency of activated carbon/magnetite nanoparticles composites in copper removal: Industrial waste recovery, green synthesis, characterization, and adsorption-desorption studies. Microporous Mesoporous Mater 311:110692

Sitko R, Turek E, Zawisza B, Malicka E, Talik E, Heimann J, Gagor A, Feist B, Wrzalik R (2013) Adsorption of divalent metal ions from aqueous solutions using graphene oxide. Dalt Trans 42:5682. https://doi.org/10.1039/c3dt33097d

Streat M, Hellgardt K, Newton NLR (2008) Hydrous ferric oxide as an adsorbent in water treatment. Process Saf Environ Prot 86:21–30. https://doi.org/10.1016/j.psep.2007.10.009

Tahoon MA, Siddeeg SM, Salem Alsaiari N, Mnif W, Ben Rebah F (2020) Effective heavy metals removal from water using nanomaterials: a review. Processes 8:645. https://doi.org/10.3390/pr8060645

Tamez C, Hernandez R, Parsons JG (2016) Removal of Cu (II) and Pb (II) from aqueous solution using engineered iron oxide nanoparticles. Microchem J 125:97–104. https://doi.org/10.1016/j.microc.2015.10.028

Taylor AA, Tsuji JS, Garry MR, McArdle ME, Goodfellow WL, Adams WJ, Menzie CA (2020) Critical review of exposure and effects: implications for setting regulatory health criteria for ingested copper. Environ Manage 65:131–159. https://doi.org/10.1007/s00267-019-01234-y

Tong S, von Schirnding YE, Prapamontol T (2000) Environmental lead exposure: a public health problem of global dimensions. Bull World Health Organ 78:1068–1077. https://doi.org/10.1590/S0042-96862000000900003

Valle JP, Gonzalez B, Schulz J, Salinas D, Romero U, Gonzalez DF, Valdes C, Cantu JM, Eubanks TM, Parsons JG (2017) Sorption of Cr(III) and Cr(VI) to $K_2Mn_4O_9$ nanomaterial a study of the effect of pH, time, temperature and interferences. Microchem J. https://doi.org/10.1016/j.microc.2017.04.021

Vamvakidis K, Kostitsi T-M, Makridis A, Dendrinou-Samara C (2020) Diverse surface chemistry of cobalt ferrite nanoparticles to optimize copper(II) removal from aqueous media. Materials 13:1537. https://doi.org/10.3390/ma13071537

Wang S, Soudi M, Li L, Zhu Z (2006) Coal ash conversion into effective adsorbents for removal of heavy metals and dyes from wastewater. J Hazard Mater 133:243–251. https://doi.org/10.1016/j.jhazmat.2005.10.034

Wang SG, Gong WX, Liu XW, Yao YW, Gao BY, Yue QY (2007) Removal of lead(II) from aqueous solution by adsorption onto manganese oxide-coated carbon nanotubes. Sep Purif Technol 58:17–23. https://doi.org/10.1016/j.seppur.2007.07.006

Wang M, Zhang Q, Hao W, Sun Z-X (2011) Surface stoichiometry of zinc sulfide and its effect on the adsorption behaviors of xanthate. Chem Cent J 5:73. https://doi.org/10.1186/1752-153X-5-73

Wang X, Huang H, Liang B, Liu Z, Chen D, Shen G (2013) ZnS nanostructures: synthesis, properties, and applications. Crit Rev Solid State Mater Sci 38:57–90. https://doi.org/10.1080/10408436.2012.736887

Wang H, Gao B, Wang S, Fang J, Xue Y, Yang K (2015a) Removal of Pb(II), Cu(II), and Cd(II) from aqueous solutions by biochar derived from KMnO4 treated hickory wood. Bioresour Technol 197:356–362. https://doi.org/10.1016/j.biortech.2015.08.132

Wang X, Chen Z, Yang S (2015b) Application of graphene oxides for the removal of Pb(II) ions from aqueous solutions: experimental and DFT calculation. J Mol Liq 211:957–964. https://doi.org/10.1016/j.molliq.2015.08.020

Wang R, Lin J, Huang S-H, Wang Q-Y, Hu Q, Peng S, Wu L-N, Zhou Q-H (2021) Disulfide cross-linked poly(methacrylic acid) iron oxide nanoparticles for efficiently selective adsorption of Pb(II) from aqueous solutions. ACS Omega 6:976–987

WHO (2003) Lead in drinking-water. Guidel Drink Qual. https://doi.org/10.1155/2013/959637

Wu W, Yang Y, Zhou H, Ye T, Huang Z, Liu R, Kuang Y (2013) Highly efficient removal of Cu(II) from aqueous solution by using graphene oxide. Water Air Soil Pollut 224:1372. https://doi.org/10.1007/s11270-012-1372-5

Yang J, Hou B, Wang J, Tian B, Bi J, Wang N, Li X, Huang X (2019) Nanomaterials for the removal of heavy metals from wastewater. Nanomaterials 9:424. https://doi.org/10.3390/nano9030424

Yin L, Wang D, Huang J, Cao L, Ouyang H, Yong X (2016) Morphology-controllable synthesis and enhanced photocatalytic activity of ZnS nanoparticles. J Alloys Compd 664:476–480. https://doi.org/10.1016/j.jallcom.2015.10.281

Zepeda AM, Gonzalez D, Heredia LG, Marquez K, Perez C, Pena E, Flores K, Valdes C, Eubanks TM, Parsons JG, Cantu J (2018) Removal of $Cu^{2+}$ and $Ni^{2+}$ from aqueous solution using $SnO_2$ nanomaterial effect of: pH, time, temperature, interfering cations. Microchem J. https://doi.org/10.1016/j.microc.2018.05.020

Zou W, Han R, Chen Z, Jinghua Z, Shi J (2006) Kinetic study of adsorption of Cu(II) and Pb(II) from aqueous solutions using manganese oxide coated zeolite in batch mode. Colloids Surf A Physicochem Eng Asp 279:238–246. https://doi.org/10.1016/j.colsurfa.2006.01.008